Formation of Banded Textures in Liquid Crystalline Polymers with Extended Curvature Elasticity

A. J. Guenthner and T. Kyu*

Department of Polymer Engineering, The University of Akron, Akron, OH 44325-0301

Received December 27, 1999

ABSTRACT: A new theoretical approach which describes the formation of banded textures in liquid crystalline polymers is introduced. The approach incorporates the concept of extended curvature elastic free energy in describing the response of the director field to strain recovery. Physically, this corresponds to accounting for an additional energetic penalty for deformation of the director field over very short distances, resulting from the natural persistence of orientation in rigid polymer chains. Both analytical and numerical results indicate that periodic patterns are spontaneously generated whenever the magnitude of the second-order gradient terms exceeds a critical value. Numerical investigations of two-dimensional systems reveal that elastic anisotropy has a significant effect on the aspect ratio and orientation of the patterns formed.

1. Introduction

It is a well-established fact that the behavior of liquid crystalline polymers (LCPs) is characterized by a wide variety of unexpected phenomena, many of which remain unexplained. One of the most intriguing phenomena associated with LCPs is the observation of "banded textures" during and after shear or elongational flow.[1] The appearance of these structures is the result of the creation of a sinusoidal or zigzag director profile along the direction of flow.[2−4] The formation of these structures has been shown to significantly affect the mechanical properties of liquid crystalline polymer fibers[5] and films[6] and is an important consideration in processes such as extrusion[7] and injection molding.[8]

Banded textures can form in many different circumstances, and although there are broad similarities between these structures, the different mechanisms responsible for their formation result in very different behaviors. Therefore, it is important to distinguish exactly which "banded texture" is being considered, since failure to do so inevitably results in further confusion of the overall picture. In this paper, a new mechanism for the formation of the banded textures observed immediately after the cessation of shear at high shear rates (where significant alignment of the LCP material is achieved) is described. It is under these circumstances that the formation of banded textures has been perhaps the least well explained and, therefore, where a significant opportunity to investigate new ideas exists.

Because many different suggestions as to the origin of the banded textures that appear after cessation of high-speed flow in LCPs have been offered, it is difficult to know which aspects of the formation process investigators should focus on. Therefore, an important contribution of any new model would be to demonstrate which properties of LCPs are crucial to the texture formation process and therefore deserve further investigation. Moreover, an understanding of why such banded textures tend to form in LCPs but not small molecule liquid crystals or flexible polymers would be very useful for the design of new materials based on liquid crystals.

The most well-known publication on this subject is the work of Kiss and Porter,[9] who studied films of poly(γ-benzyl-glutamate) (PBG) solutions in *m*-cresol. Many of the studies of banded textures in LCPs in the following years included observations of patterns formed after cessation of high-speed flow,[10−18] although some materials, most notably anisotropic solutions of PBG, did not consistently form banded textures under these particular circumstances.[19] On the other hand, it has been shown for liquid crystalline solutions of both poly(*p*-phenylene terephthalamide) (PPTA)[20] and natural silk[14] that this type of banded texture can be either eliminated or made to appear as a result of physical processing of the material. Therefore, a proper understanding of the mechanism of formation for these patterns should have important consequences for the processing of LCPs as well as the development of new materials.

Over the years a number of suggestions as to the source of banded texture have focused on compressive stresses in LCPs.[15] Recently Vermant and co-workers[19] suggested the contraction of stretched twist disclination loops as the source of such stresses, and Fisher, Keller, and Windle[23] suggested that the director field experiences buckling under compressive stresses which appear after cessation of flow. The source of these stresses was postulated to be some form of network structure within the material. Further work by Windle[24] has shown that the dynamic viscoelastic characteristics of LCPs are indeed consistent with the presence of a network structure.

Although the molecules of liquid crystalline polymers are generally thought of as existing in an extended conformation, the nature of the entangled network which permits the transfer of elastic stresses in the material has received increasing attention recently.[18] Since it has been shown both theoretically[26] and experimentally[27] that LCPs of sufficiently high molecular weight will adopt a biased random coillike conformation, the existence of linear entanglements in LCPs is quite probable. A network structure will impart a degree of

* To whom correspondence should be addressed. E-mail: tkyu@uakron.edu.

10.1021/ma9921448 CCC: $19.00
Published on Web 06/13/2000

elasticity to the material that would not be expected if the molecules adopted a simple extended conformation. The effects of this elasticity must be taken into account in order to understand the dynamics of LCPs during the formation of banded textures.

The idea that LCPs experience stress relaxation after cessation of shear is well accepted. In fact, the formation of the banded structure has even been associated with a specific phase of stress relaxation following flow in nematic solutions of the rigid rod polymer poly(1, 4-phenylene-2,6-benzobisthiazole) (PBZT).[28] However, why the structure should relax to a periodic state is not well understood. In low molecular weight liquid crystals, periodic structures often form as part of a transient response during reorientation induced by external fields.[29] After a short time, though, these structures disappear in favor of a "domain wall" texture. In contrast, the periodic structures that form in LCPs are known to be much more stable.[30] Although stable periodic structures can form in LCPs for a number of reasons, including the presence of a high degree of elastic anisotropy when splay−twist deformation is involved, as pointed out by Meyer,[31] the resultant texture is a set of stripes that run parallel to the director and therefore does not explain the banded textures associated with cessation of shear flow, which are aligned perpendicular to the director and involve mainly bend deformation. Thus, an important element in any model of banded texture formation should be the mechanism by which stress relaxation can lead to stable periodic textures such as those observed experimentally after cessation of flow.

In addition, any investigation of pattern formation in liquid crystalline polymers must take into account the fact that the orientation of the director is very often nonuniform under quiescent conditions. Therefore, the possibility that a preexisting structure is responsible for the formation of the banded texture must be considered. Even though this is indeed the case for banded textures that form after flow at low strain rates,[19] two important observations make it unlikely that the same mechanism is at work in cases involving high-speed flows. The first is the well-known tendency for the orientational heterogeneity in liquid crystalline polymers to disappear during flow if the rate of strain is sufficiently large.[32,33] The second is the observation by Srinivasarao and Berry[34] that banded textures in PBZT solutions formed after high-speed shearing of samples that were carefully prepared so as to have an initially uniform orientation of the director. Ideally, any model of banded texture formation in LCPs should be able to explain the observed patterns which arise when no initial texture is present while retaining the ability to describe the transformation of preexisting structures into banded textures along the lines of existing theories.

2. Model for LCP Reorientation Dynamics

2.1. Development of the Model. Since the formation of banded textures after cessation of shear is associated with dynamic phenomena, a clearer picture of why these patterns form can only be obtained if the reorientation dynamics of the LCP director field are studied. These dynamics are at least partially governed by the elastic free energy, which in liquid crystals is traditionally given by the Frank free energy.[35] This free energy is based on the concept of curvature elasticity, in which the first spatial derivatives of the director field (known as curvature strains) are assumed to play a role similar to ordinary strains in elastic materials. The Frank free energy (F_{ce}) is given by the expression

$$F_{ce} = \int_V \left\{ \frac{1}{2}[k_1(\nabla \cdot \mathbf{n})^2 + k_2(\mathbf{n} \cdot \nabla \times n)^2 + k_3(\mathbf{n} \times \nabla \times \mathbf{n})^2] \right\} dV \quad (1)$$

where the parameters k_1, k_2, and k_3 are referred to as splay, twist, and bend elastic constants, respectively, and where the unit vector $\mathbf{n}$ represents the liquid crystal director.

The Frank free energy provides an adequate description of curvature elasticity in low molecular weight liquid crystals. However, it is important to consider whether the Frank free energy is capable of adequately describing curvature elasticity in LCPs. The Frank free energy is based on the traditional continuum description of liquid crystalline materials which requires an "elementary volume" composed of many chain segments that can behave independently of each other, that is, longer than the persistence length of the chain in the nematic state. However, the banded textures that appear in LCP materials can have periodicities as small as 500 nm,[36] which is not much larger than the persistence length of many LCPs in the nematic state (around 30 nm for PPTA fibers).[37] As a result, it is clearly difficult to fully satisfy the assumptions of a traditional continuum theory in this case.

However, it is possible to describe the formation of banded textures using a modified continuum theory which does not require chain segments with independent orientations. Although this situation is mathematically complex, one very simple means of approximating the distance-dependent correlation between chain segments is to incorporate higher-order gradient terms in the curvature elastic free energy.[38] This is the equivalent of a lattice model in which not only nearest neighbors, but also second-nearest neighbors influence the orientation. The resulting free energy functional (which will be referred to as the extended Frank free energy) takes the form

$$F_{ce} = \int_V \left\{ \frac{1}{2}[k_{ijlm} \nabla_i n_j \nabla_l n_m + \epsilon_{pqrstu} \nabla_{pq} n_r \nabla_{st} n_u] \right\} dV \quad (2)$$

where k_{ijlm} and ϵ_{pqrstu} are referred to as first-order and second-order curvature elastic constants (with representative magnitudes k and ϵ) for clarity. The last term in the above expression imposes an additional energetic penalty for deforming the material over small length scales. This additional penalty becomes significant when the deformation occurs over length scales less than $(\epsilon/k)^{1/2}$. The result is an extended curvature elasticity in which deformations over distances smaller than $(\epsilon/k)^{1/2}$ tend to be suppressed more than normal, corresponding to the effects of chain rigidity. In multidimensional cases, this quantity should be anisotropic since the persistence of orientation in directions perpendicular to polymer chains should be much less than in directions along the chain.

To reveal whether the use of the extended Frank free energy has any significance in explaining the formation of banded textures, the reorientation dynamics of the director field must be investigated. The investigation must also include the effects of stress relaxation after cessation of flow in LCPs due to ordinary (rubberlike)

elasticity. This stress relaxation should be accompanied by strain recovery. One means by which strain recovery can occur would be by affine center-of-mass motion of the material. Such motion involves the bulk flow of LCP material accompanied by a reduction in the overall local orientation, and has been observed to occur on time scales of tens to hundreds of minutes after cessation of flow,[28] which is much longer than the time scale associated with the formation of banded textures.

Another means by which strain recovery can occur is a local rotation of the director field. Since the director field is based on the direction of orientation of physical chain segments, a rotation of the field must correspond to an overall rotation of physical elements. If these elements experience a net rotation away from the direction of flow, then the overall dimensions of the material in the flow direction will be reduced. In addition, the rotation would generate backflow in order to maintain a constant density. Because of this backflow, the deformation would not be affine. If the deformation involved is small and occurs slowly, however, the backflow will be almost completely confined to directions perpendicular to the direction of strain recovery[32] and its impact on the reorientation of the director will be small. Under these circumstances, we can link the director field (which is considered incompressible) to the strain in the material (denoted by λ) by writing

$$\lambda/\lambda_{r0} = n_2 \tag{3}$$

where λ_{r0} represents the initial value of the recoverable strain at the beginning of the reorientation and z is the direction of the strain (thus, initially $n_z = 1$). If a simple neo-Hookean potential (in planar uniaxial extension, for instance) is used, the result is

$$F_{el} = \sum_V \{W[(\lambda_{r0} n_z)^2 + 1/(\lambda_{r0} n_z)^2 - 2]\}\, dV \tag{4}$$

where W is the ordinary elastic modulus. The total free energy is then the sum of the extended curvature elasticity and the ordinary elasticity, or

$$F = \int_V \left\{\frac{1}{2}[k_{ijlm}\nabla_i n_j \nabla_l n_m + \epsilon_{pqrstu}\nabla_{pq} n_r \nabla_{st} n_u] + W[(\lambda_{r0} n_z)^2 + 1/(\lambda_{r0} n_z)^2 - 2]\right\} dV \tag{5}$$

A system governed by this type of free energy functional will attempt to relieve strain energy by reorienting the director field. Although in reality the coupling between the director field and strain recovery can be much more complicated, this simplified model should suffice to at least capture the qualitative behavior of the system when the amount of reorientation is small.

Although the model derived so far is a general multidimensional one, the number of parameters it contains is potentially enormous. However, it is possible to reduce the number of parameters by considering the symmetries of LCP materials, especially in the nematic state. If a two-dimensional system is considered, then in the case of first order curvature elasticity, there are only two basic deformation types (splay and bend), with moduli represented by k_1 and k_3, respectively. For second-order curvature elasticity, only three basic types (with moduli represented by ϵ_{11}, ϵ_{13}, and ϵ_{33}) exist. In vector form the curvature elastic free energy, F_{ce}, is given by

$$F_{ce} = \int_V \left\{\frac{1}{2}\begin{bmatrix} k_1(\nabla\cdot\mathbf{n})^2 + k_3(\mathbf{n}\times\nabla\times\mathbf{n})^2 + \\ \epsilon_{11}[\mathbf{n}\times\nabla\times\mathbf{n}(\nabla\cdot\mathbf{n}) - 2(\mathbf{n}\times\nabla\times\mathbf{n})(\nabla\cdot\mathbf{n})]^2 + \\ \epsilon_{13}[\nabla\cdot\mathbf{n}(\nabla\cdot\mathbf{n}) - (\nabla\cdot\mathbf{n})^2 + (\mathbf{n}\times\nabla\times\mathbf{n})^2]^2 + \\ \epsilon_{33}[\mathbf{n}\times\nabla\times\mathbf{n}\times\nabla\times\mathbf{n} + 2(\mathbf{n}\times\nabla\times\mathbf{n})(\nabla\cdot\mathbf{n})]^2 \end{bmatrix}\right\} dV \tag{6}$$

For simplicity the director may be represented by a single angle θ which measures the deviation from the direction of flow. This allows the following expression for the curvature elastic free energy to be developed:

$$F_{ce} = \int_V \left\{\frac{1}{2}\left[p_{ij}(\theta)\frac{\partial\theta}{\partial x_i}\frac{\partial\theta}{\partial x_j} + q_{klmn}(\theta)\frac{\partial^2\theta}{\partial x_k \partial x_l}\frac{\partial^2\theta}{\partial x_m \partial x_n}\right]\right\} dV \tag{7}$$

Here, the functions $p_{ij}(\theta)$ and $q_{klmn}(\theta)$ depend on the given coordinate system. For instance if $\theta = 0$ corresponds to the direction of alignment, then $p_{11}(\theta) = k_1 \sin^2\theta + k_3 \cos^2\theta$ and $q_{1111} = \epsilon_{11}\sin^4\theta + \epsilon_{13}\sin^2\theta\cos^2\theta + \epsilon_{33}\cos^4\theta$.

Since initially the direction of strain corresponds to the direction of initial alignment (that is, $\theta = 0$), then $n_z = \cos\theta$, and, for planar uniaxial extension

$$F_{el} = \int_V [W(\lambda_{r0}{}^2\cos^2\theta + 1/(\lambda_{r0}{}^2\cos^2\theta) - 2)]\, dV \tag{8}$$

We can further simplify matters by introducing a small angle approximation, namely, $\cos\theta \approx 1 - \theta^2/2$, and therefore $1/\cos\theta \approx 1 + \theta^2/2$. Then, by introducing the variable $\psi = 4(\lambda_{r0} - 1)$, given that if the angle θ is small, then the recoverable strain must be small as well, we can write, $\lambda_{r0}{}^2 = (1 + \psi/4)^2 \approx 1 + \psi/2$, and $1/\lambda_{r0}{}^2 \approx (1 - \psi/4)^2 \approx 1 - \psi/2$, so that, after substitution, eq 8 becomes:

$$F_{el} = \int_V \{W\left[\left(\frac{1}{4}\theta^4 - \theta^2 + 1\right)(1 + \psi/2) + \left(\frac{1}{4}\theta^4 + \theta^2 + 1\right)(1 - \psi/2 - 2]\right\} dV$$

or

$$F_{el} = \int_V \left[W\left(\frac{1}{2}\theta^4 - \psi\theta^2\right)\right] dV \tag{9}$$

Note that this form represents a simple symmetric double-well potential with a maximum at $\theta = 0$ and minima at $\theta = \pm\psi^{1/2}$.

Given the free energy functional, the equation of motion for the system can be written using the time-dependent Ginzburg−Landau (TDGL) equation. The curvature elastic part of the equation of motion is given by

$$\gamma\frac{\partial\theta_{ce}}{\partial t} = -p'_{ij}(\theta)\frac{\partial\theta}{\partial x_i}\frac{\partial\theta}{\partial x_j} + p_{ij}(\theta)\frac{\partial^2\theta}{\partial x_j \partial x_j} + q'_{klmn}(\theta)\frac{\partial^2\theta}{\partial x_k \partial x_l}\frac{\partial^2\theta}{\partial x_m \partial x_n} - q_{klmn}(\theta)\frac{\partial^4\theta}{\partial x_k \partial x_l \partial x_m \partial x_n} \tag{10}$$

where the primes denote differentiation with respect to θ. The ordinary elastic part of the equation of motion is given by

$$\gamma\frac{\partial\theta_{el}}{\partial t} = 2W[\psi\theta - \theta^3] \tag{11}$$

These two can be added together to form a partial differential equation which may be solved by analytical methods in very simple cases or by using an appropriate numerical technique for more complex cases. The solution is then the time-dependent behavior of the system, from which key characteristics may be extracted as a function of the system parameters.

2.2. Analysis for the One-Dimensional Case. For the purposes of analysis, a simple one-dimensional version of eqs 7 and 9 with the one-constant approximation for Frank elasticity can be written as

$$F = \int_V \left\{ \frac{1}{2}\left[k\left(\frac{\partial\theta}{\partial x}\right)^2 + \epsilon\left(\frac{\partial^2\theta}{\partial x^2}\right)^2 \right] + W\left(\frac{1}{2}\theta^4 - \psi\theta^2\right) \right\} \mathrm{d}V \quad (12)$$

The resulting equation of motion is then

$$\gamma\frac{\partial\theta}{\partial t} = k\frac{\partial^2\theta}{\partial x^2} - \epsilon\frac{\partial^4\theta}{\partial x^4} + 2W[\psi\theta - \theta^3] \quad (13)$$

which can be normalized to give

$$\frac{\partial\theta}{\partial\tau} = \frac{\partial^2\theta}{\partial X^2} - \beta\frac{\partial^4\theta}{\partial X^4} + \theta - \frac{\theta^3}{\psi} \quad (14)$$

with the dimensionless parameters, $\tau = (2W\psi/\gamma)t$, $X^2 = (2W\psi/k)x^2$, and $\beta = 2W\psi\epsilon/k^2$.

Equation 14 is actually a slightly modified form of the extended Fisher−Kolmogorov (EFK) equation.[40,41] The behavior of this equation has been analyzed both physically and mathematically. The most important result of this analysis has been to confirm that periodic solutions of the homogeneous version of this equation do exist if the dimensionless parameter β exceeds a critical value;[42] otherwise, the system displays the solitary wave behavior typical of the traditional Fisher−Kolmogorov equation.[43] Moreover, the dynamics of this equation have been examined in the context of the marginal stability hypothesis[44−47] in order to provide an estimate of both the speed at which a periodic pattern propagates across the system and the associated periodicity as a function of β. These analyses also predict the formation of a pattern with a uniform periodicity that eventually remains constant over time by a dynamic selection mechanism. Another important implication of the above analysis comes from the work of Aronson and Weinberger,[48] which shows that for similar equations the qualitative behavior of the system is the same for almost any function that is qualitatively similar to the last two terms of eq 14. This means that the behavior displayed by the system is insensitive to the exact details of the regular elastic strain energy function and its coupling to the director field, thus the approximate treatment given above should suffice to capture qualitatively the system behavior.

3. Numerical Analysis Procedure

3.1. Simulation Method. Since banded textures are multidimensional patterns, a more complete model of their formation should involve at least two dimensions. Investigating the behavior of these models requires numerical solutions for the multidimensional form of eq 14, because the ability to analytically solve the multidimensional equations is extremely limited. To obtain the time-dependent numerical solutions, a finite difference scheme in two dimension was employed using Euler's method with central spatial differences. Both the grid spacing and the time step were maintained at values that were sufficiently small to ensure that changes in them had only a slight influence on the results. Moreover, quantitative information, such as the propagation velocities of the patterns, was always obtained by running simulations at the same Courant number ($\Delta\tau/\Delta X^2$) but different grid spacings (ΔX) and extrapolating to $\Delta X = 0$, keeping in mind that the errors obtained using central differences are $O(\Delta X)^2$. In addition, a few simulations were carried out using the more complex alternating directional implicit method with similar grid sizes and time steps in order to determine whether the results depended on the simulation scheme. The results of these simulations were found to be nearly identical to those carried out using Euler's method under the same conditions.

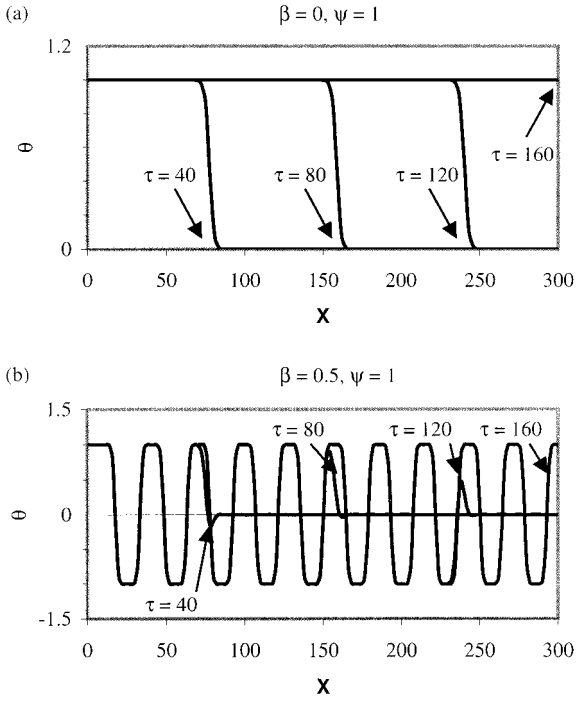

Figure 1. One-dimensional profile of the evolution of the director governed by the extended Frank free energy. (a) When $\beta = 0$, a propagating solitary wave results; (b) when $\beta = 0.5$, a periodic pattern forms. The arrows indicate the location of the leading edge of the wave front at various values of τ. In both cases, $\theta = 0$ at $\tau = 0$ throughout the system.

3.2. Validation of the Method. Although it is difficult to establish the validity of the complex multidimensional solutions of eq 14 directly, the results of the model in the one-dimensional case can be used to test the accuracy of the numerical technique. By introducing a disturbance uniformly along one edge of the grid and using no-flux boundary conditions along with the one-constant approximation for curvature elasticity, the patterns which form vary only along the direction perpendicular to the line of disturbance; hence, they may be compared to results obtained using the analytical methods discussed earlier. These methods may be used to compute the propagation velocity of the pattern as a function of β, the value of β at which the transition to periodic pattern formation takes place, and the wavelength of any periodic patterns formed.

The most important of these quantities is the critical value of β for periodic pattern formation. This value may be determined approximately by simply examining the behavior of the system over a wide range of β values. For instance, in Figure 1a, a one-dimensional view of the director pattern at various times is shown for the case $\beta = 0$. As can be seen, the system is transformed from the unstable orientation at $\theta = 0$ to a stable orientation at $\theta = 1$. In Figure 1b, the value of β is 0.5, and now the pattern which propagates through the system is periodic. However, because the wavelength of the pattern is predicted to become infinitely large near the transition point, a more sophisticated method for detecting the transition is needed. Such a method is demonstrated in Figure 2a, which

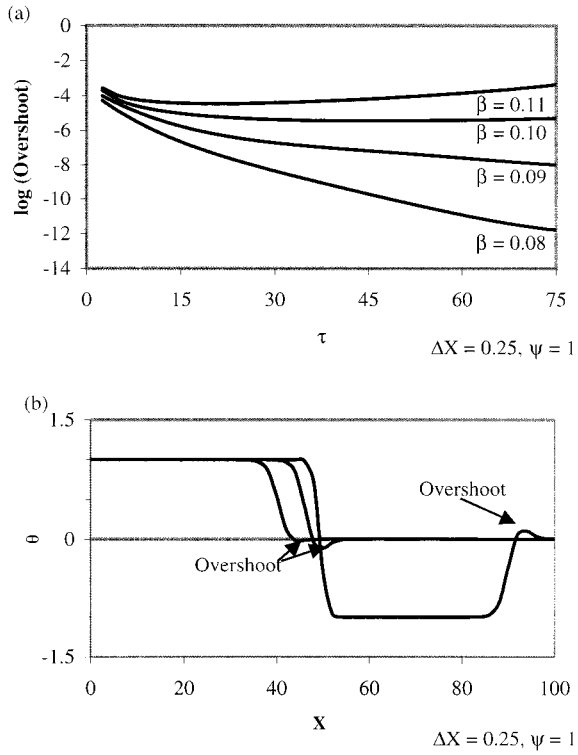

Figure 2. Evolution of the director profile for nonzero values of β. (a) The magnitude of the overshoot as a function of X ($\Delta X = 0.25$) showing that between $\beta = 0.09$ and 0.1, a transition from a damped overshoot to a growing overshoot takes place. The result is the periodic pattern illustrated in part b. Extrapolation to $\Delta X = 0$ gives $\beta = 0.096$ for the transition to periodic pattern formation.

shows the maximum value of the overshoot (depicted schematically in Figure 2b) in a propagating pattern plotted as a function of position for different values of β. At low values of β, any initial transient overshoot rapidly decays, but when β reaches a value of 0.09−0.1, the overshoot decays but then begins to grow again, indicating a loss of stability in the traveling wave and the onset of periodic pattern formation.

To predict analytically when this transition will occur in a dynamic system, the marginal stability hypothesis can be employed. This hypothesis allows the properties of the propagating fronts in the system to be determined from a simplified analysis of the behavior at the leading edge of the front. On the basis of this type of analysis, van Saarloos[41] determined that the dynamically selected velocity v* of a uniformly translating front for the extended Fisher−Kolmogorov equation would be

$$v^* = \frac{2}{\sqrt{54\beta}}[1 + 36\beta - (1 - 12\beta)^{3/2}]^{1/2} \qquad (15)$$

This expression, of course, holds only when $\beta < {}^1/_{12}$. For larger values of β, uniformly translating fronts are unstable. Thus, the transition to periodic pattern formation should occur at $\beta = {}^1/_{12}$. For $\beta > {}^1/_{12}$, the velocity of the envelope containing the periodic pattern is given by

$$v^* = \left[\frac{4}{3} + \frac{5}{18\beta} - \frac{1}{18\beta}\sqrt{7 + 24\beta}\right]\left[\frac{1 + \sqrt{7 + 24\beta}}{24\beta}\right]^{-1/2} \qquad (16)$$

The numerically observed propagation velocity, which may be computed either by a front tracking method, or in the case of solitary waves, by examining the rate of energy dissipation in the system, is compared to the values predicted by the marginal stability analysis in Figure 3a. These values agree to within an average of 0.6% over the entire range of β which was examined.

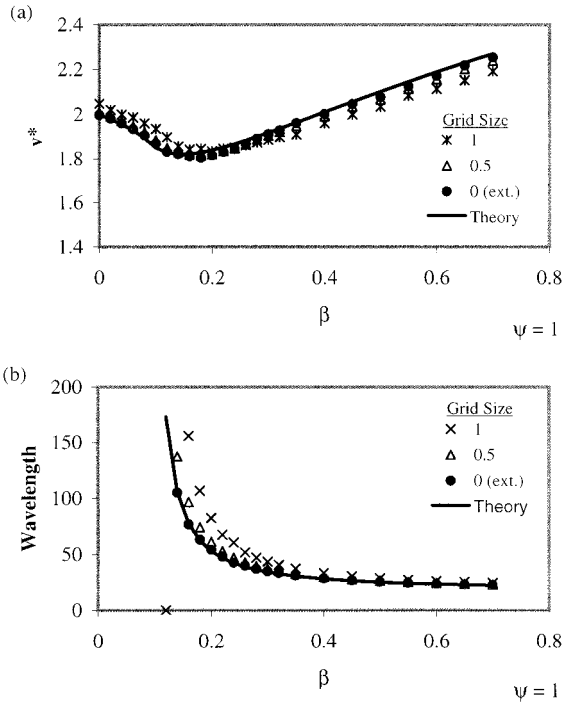

Figure 3. Characteristics of the periodic patterns formed in one-dimensional systems: (a) the propagation velocity and (b) the selected wavelength as functions of β. The solid lines represent the predictions based on the marginal stability hypothesis, while the symbols represent the results of simulations with varying grid sizes. The filled circles show the results when extrapolated to zero grid size, which agree with the theoretical values to within 2%.

The wavelength of the periodic pattern can be predicted using a different form of marginal stability analysis given by Ben-Jacob and co-workers.[45] Specifically, the wavevector of the selected pattern at the leading edge of the front can be found by solving the equations

$$\frac{d\omega}{dq} = ic \qquad \text{and} \qquad \mathrm{Re}[\omega'(q)] = 0 \qquad (17)$$

where $\omega'(q) = \omega(q) - icq$, c is the selected velocity of the leading edge of the front, and $\omega(q)$ is given by the linear dispersion relationship of the equation around the point $\theta = 0$. Using the combination of c and q which satisfies eq 17, the wavelength q^* of the selected pattern is given by

$$q^* = 1/c\ \mathrm{Im}[\omega(q)] \qquad (18)$$

In Figure 3b, the wavelength of the patterns produced by numerical solution are compared with the values obtained using eqs 17 and 18. The discrepancy is 1.7% on average, although testing at the very longest wavelengths was not attempted due to the extremely large simulation regions and long running times required. Moreover, the numerically observed wavelength rapidly becomes constant over time as predicted by the marginal stability hypothesis. Altogether, these results demonstrate that the observed patterns are consistent with predictions based on well-established principles of nonlinear dynamics. They therefore lend credence to the numerical solutions obtained in more complex two-dimensional cases.

4. Results and Discussion

4.1. Effect of "First-Order" Elastic Anisotropy. In the two-dimensional case, there will be two "first-order" elastic constants and three "second-order" elastic constants, producing both "first-order" and "second-

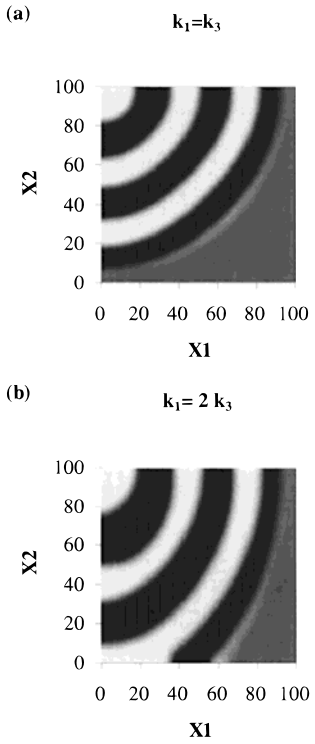

Figure 4. Two-dimensional pattern formed at $\tau = 50$ for (a) both first and second-order elastic isotropy and (b) $k_1 = 2k_3$ with second-order isotropy ($\beta = 0.5$). Initially, the directors all point in the X1 direction. A disturbance was introduced in the upper left corner at $\tau = 0$. Darker shades represent a more negative X2 components of the director, while lighter shades indicate a more positive X2 component, with grays representing a director with a near zero X2 component (therefore along X1).

order" elastic anisotropy. This elastic anisotropy can significantly influence the behavior of the system. First-order elastic anisotropy is attributed to the difference in free energy needed to produce splay and bend deformation in LCPs. As the molecular weight of the LCP molecules increases, the ratio k_1/k_3 can grow quite large[49] due to the fact that splay deformation in long rigid rods requires a considerable change in density, adding a significant energy cost to splay deformation relative to bend deformation.[50] The effects of first-order anisotropy on pattern formation are 2-fold. First, the system will tend to avoid splay whenever possible, creating a director field in which bend is more prevalent than in results obtained using the one-constant approximation. Second, the velocity of wave propagation will depend on the direction of propagation. On the basis of dimensional analysis, the propagation velocity should be proportional to $k\gamma/W^{3/2}$. For propagation parallel to the director, $k = k_3$, while for propagation perpendicular to it, $k = k_1$. Since $k_1 \gg k_3$, the wave will propagate much faster in the direction perpendicular to the director. The result is a texture that is elongated in the direction perpendicular to the director. This effect can be demonstrated for periodic patterns using simulations of the normalized versions of eqs 10 and 11. In Figure 4a, $k_1 = k_3$ (first-order elastic isotropy) and $\epsilon_{13} = 2\epsilon_{11} = 2\epsilon_{33}$ (second-order elastic isotropy), with $\beta = 0.5$ in all directions. The resulting pattern is a series of concentric rings, as expected for an isotropic system with a point disturbance. In Figure 4b, $k_1 = 2k_{33}$ (first-order elastic anisotropy) but the value of β is the same (0.5) in all directions (second-order elastic isotropy). The resulting pattern is a series of concentric ovals, with an eccentricity of about 1.4. This result is consistent with dimensional analysis, which indicates that the eccentricity should be proportional to the square root of the first-order elastic anisotropy in such a system.

4.2. Effect of "Second-Order" Elastic Anisotropy. It is apparent that second-order anisotropy can also influence the pattern-forming behavior of the system. However, the critical parameter in this case will be the normalized second-order elastic constants (β's) rather than the actual values of ϵ_{11}, ϵ_{33}, and ϵ_{13}. Note: $\beta_{11} = 2W\psi\epsilon_{11}/k_1^2$, $\beta_{13} = 2W\psi\epsilon_{13}/k_1\ k_3$, and $\beta_{33} = 2W\psi\epsilon_{33}/k_3^2$. Second-order elastic anisotropy may be described as the result of a differing set of energy penalties for various forms of deformation associated with the second-order gradients of the director field. However, this approach is quite complicated and difficult to visualize. A more understandable approach to second-order elastic anisotropy arises from the physical interpretation of the origin of the higher-order gradient terms in the curvature elastic free energy expression. These terms are due to the distance-dependent orientational correlation in the director field that results from the large persistence length associated with LCPs. In the liquid crystalline state, however, the persistence length will show a dependence on direction. Specifically, for main-chain nematic LCPs, the persistence length will be largest in the direction parallel to the director (large ϵ_{33} compared to ϵ_{11} and ϵ_{13}).

The effects of second-order elastic anisotropy on the pattern formation process are shown in Figure 5, parts a−c, in which $k_1 = k_3$, but only one of the second-order terms (β_{33} in Figure 5a, β_{11} in Figure 5b, and β_{13} in Figure 5c) is nonzero. The figures clearly show that the direction of the bands depends on the second-order elastic anisotropy. These results can be understood in terms of the propagation of pattern forming waves in the system. The nature of patterns propagating along the director is controlled primarily by β_{33}, the nature of patterns propagating perpendicular to the director is controlled primarily by β_{11}, and the nature of patterns which form perpendicular to the direction of propagation is controlled by β_{13}. Whenever the value of β for the given propagation direction is large enough, a periodic pattern emerges. Combining the results shown in Figures 4 and 5 reveals that a system in which $k_1 \gg k_3$ and $\beta_{33} \gg \beta_{11} \gg \beta_{13}$ (such as a main-chain LCP) should exhibit stripes perpendicular to the direction of alignment.

4.3. Domain Growth. So far, the patterns which have been investigated all feature a band spacing which does not increase with time. However, this is not always the case, as illustrated in Figure 6. The figure shows the evolution of the pattern formed with $k_1 = 10k_3$ and $\beta_{33} = 10\beta_{13} = 100\beta_{11}$ in the presence of a large amount of thermal noise. The instability of the initial state creates a set of elongated domains. The smaller features soon disappear from the system, since short-wavelength fluctuations are much less stable than their longer-wavelength counterparts. Then, on a much longer time scale, another transformation takes place. The curved domain walls are slowly transformed into straight ones, through a process in which any salients in the domain boundaries are removed, starting with the smaller ones and continuing through the larger ones.

The reason for this behavior is that the gradient terms in the free energy expression function in a manner

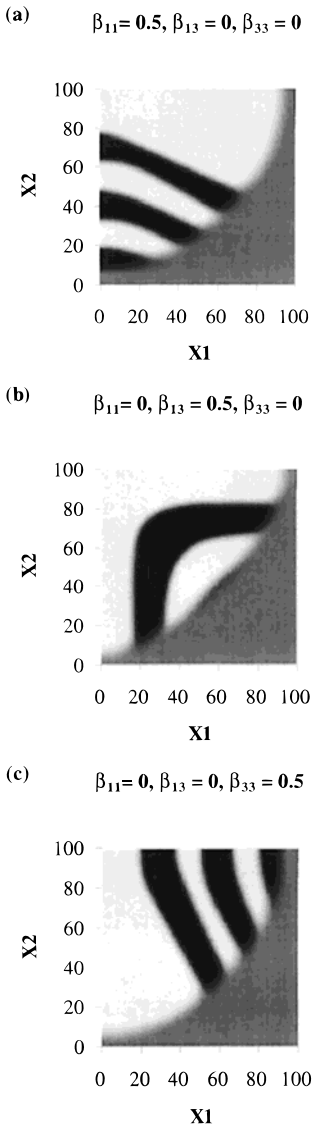

Figure 5. Effect of second-order anisotropy on pattern formation. The initial conditions are as in Figure 4, and $k_1 = k_3$ as in Figure 4a, but in part a, $\beta_{11} = 0.5$ while β_{13} and $\beta_{33} = 0$, in part b, $\beta_{13} = 0.5$ while β_{11} and $\beta_{33} = 0$, and in part c, $\beta_{33} = 0.5$ while β_{11} and $\beta_{13} = 0$. The shading is the same as in Figure 4.

analogous to interfacial energy terms. In fact the correct term for these domain boundaries is "antiphase boundaries".[51] The elimination of salients and destruction of smaller domains is then due to the tendency to minimize this "antifacial" energy. Moreover, in elastically anisotropic systems, the antifacial energy should depend on the orientation of the normal to the antiphase boundary, resulting in the tendency of retaining the antiphase boundaries that are oriented in the direction of least energy. Since the largest contributors to this antiphase energy are the first-order gradients of the director field, the antiphase boundaries produced by bend deformation should be favored over boundaries produced by splay deformation in LCPs. When the overall deformation of the director field is small, this means that antiphase boundaries running perpendicular to the director should be much more stable than those running parallel to the director field. These results are nearly identical to those obtained using the model of Picken and co-workers for relaxation of domain textures in systems described by the Frank free energy.[52] Therefore, for LCPs with a heterogeneous orientation (observed during and after

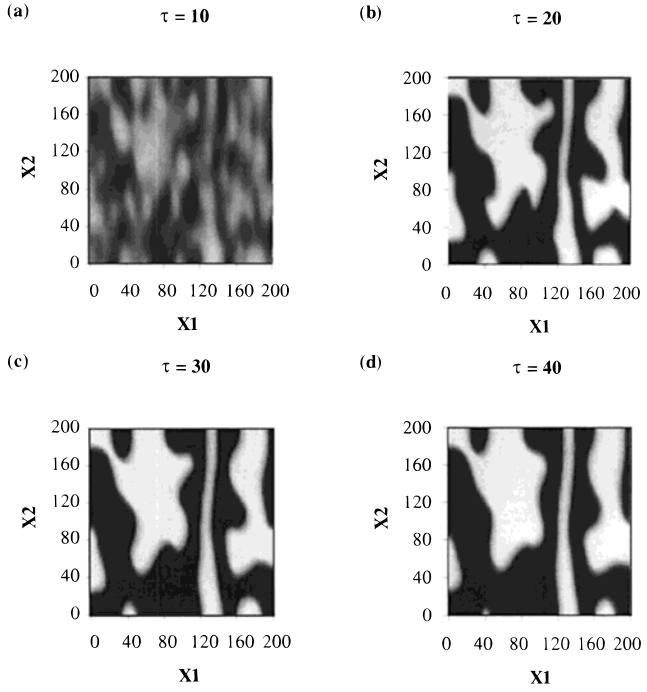

Figure 6. Evolution of a two-dimensional system ($k_1 = 10k_3$ with $\beta_{11} = 0.05$, $\beta_{13} = 0.05$, and $\beta_{33} = 0.5$) with a random initial distribution of large fluctuations about X1 in the director field: (a) $\tau = 10$, (b) $\tau = 20$, (c) $\tau = 30$, and (d) $\tau = 40$. Shading is the same as in Figures 4 and 5. Under these conditions, the average band spacing grows with time.

slow flows), the inclusion of the higher-order gradient terms would not affect the formation of banded textures through the mechanism described by Vermant and co-workers.[19] On the other hand, if the tendency to form a domain texture is suppressed (as it is in high-speed flows), a banded texture where the domains do not grow with time is formed instead. This is illustrated in Figure 7, which shows the results of a simulation identical to Figure 6 except that there is no initial domain texture. Instead the bands grow from a set of isolated initial "kink" defects in the presence of a small amount of thermal noise. The growth of these bands creates a pattern which is initially much more regular than the one shown in Figure 6. As a result, the pattern changes little once the banded texture has spread throughout the system. Hence the band spacing will remain virtually unchanged over time. The ability to capture both types of banded texture formation is a characteristic not seen in previous models.

Similar results should be obtained if the calculations were performed in three dimensions. In the three-dimensional case, the number of elastic constants will be larger, further complicating the calculations. In addition, the director field must be described by two independent quantities (such as polar and azimuthal angles). Thus, the behavior of the system will be described by two coupled nonlinear differential equations. Coupling effects in these equations can be important, as demonstrated by Lonberg and Meyer,[31] who showed that they are responsible in part for the formation of stable periodic structures in LCP films subjected to magnetic fields.

4.4. Comparison with Experimental Observations. Having demonstrated the dynamic behavior of the system in terms of the solutions of eqs 10 and 11, it is important to consider what comparisons can be made

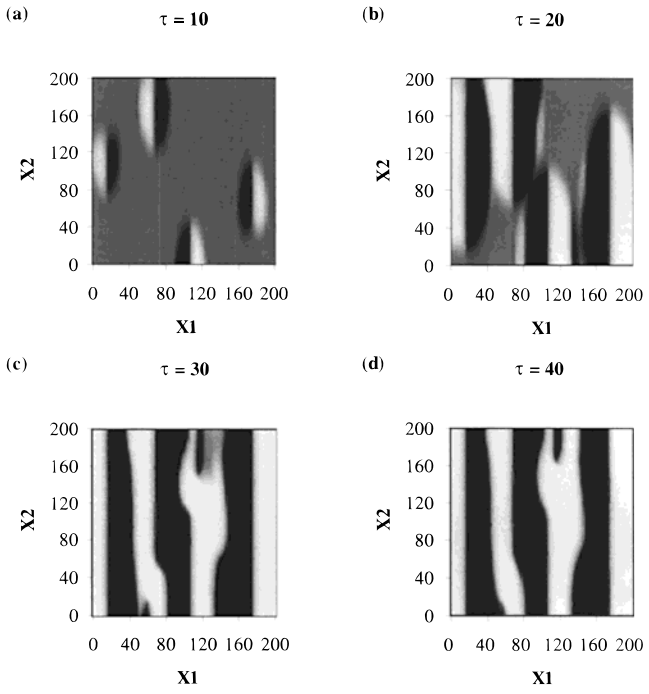

Figure 7. Evolution of a two-dimensional system ($k_1 = 10k_3$ with $\beta_{11} = 0.05$, $\beta_{13} = 0.05$, and $\beta_{33} = 0.5$) with a random initial distribution of small kink fluctuations about X1 in the director field. X1 therefore corresponds to the direction of previous shear: (a) $\tau = 10$, (b) $\tau = 20$, (c) $\tau = 30$, and (d) $\tau = 40$. Shading is the same as in Figures 4 and 5. Under these conditions, the average band spacing remains nearly constant in time.

between the behavior of the model and experimental data. One of the key predictions of the model is that the dimensionless parameter β must exceed a critical value. This dimensionless parameter is proportional to the square of the ratio of two of the characteristic length scales present in the system. The first, given by $(\epsilon/k)^{1/2}$, represents the characteristic length over which the orientation of the LCP chain segments persists. The second, given by $(k/2W\psi)^{1/2}$, is the characteristic radius of curvature (or scale of deformation) produced by the stresses present in the system. When the radius of curvature is much larger than the persistence length, β approaches zero and the Frank free energy may be used to accurately describe the curvature elastic behavior of the system.

However, for any given material, the Frank elastic constants depend on the persistence length.[53,54] If this dependence is incorporated into the expression for β, then β should increase with increasing persistence length. Thus, one prediction of the model is that a material must have a persistence length larger than a critical value in order for banded textures to form for given values of W and ψ. Moreover, since β is proportional to W, larger elastic stresses will favor the formation of banded textures. If these elastic stresses are associated with an entangled network structure, then they should be significant only when the molecular weight exceeds a critical value. Indeed a critical molecular weight threshold for the formation of banded textures after cessation of shear has recently been found[55] that corroborates earlier studies of the effect of molecular weight on banded texture formation.[56] These two facts taken together mean that only materials with sufficiently large persistence lengths and elastic stresses (such as LCPs subjected to high-speed flow) should form banded textures. Furthermore, the model predicts that when significant fluctuations of the director field are initially present, a banded texture consisting of elongated domains which grow larger with time will form, whereas if no initial domain texture is present and fluctuations are limited, a static banded texture will form. Since domain textures in LCPs tend to disappear once the shear rate is sufficient to cause flow alignment, the model suggests that banded textures with a band spacing that increases with time should emerge at low shear rates, while textures with a band spacing that is constant in time should emerge at higher shear rates. This agrees with the results of many of the domain growth experiments conducted by Vermant and coworkers.[19]

In addition to predicting the conditions under which a banded texture will form, the model also allows some approximate predictions about the characteristics of the banded texture itself, namely the orientation and size of the bands. In highly anisotropic materials, the bands always run perpendicular to the direction in which the dimensionless parameter β has the highest value, which for main-chain LCPs is parallel to the director. This is indeed a typical characteristic of banded textures which form after cessation of flow in LCPS. According to the model, the spacing of the bands should be around 20 times the characteristic length $(k/2W\psi)^{1/2}$ of the system. The order of magnitude for k is approximately 10^{-11} N for many lyotropic LCPs.[57] The order of magnitude of W should be given by the network elastic modulus of the material. Although this parameter is quite difficult to measure in samples which are subjected to very rapid flow, we can make an order of magnitude estimate based on the amount of stress relaxation and strain recovery present during band formation. Odell et al.[28] observed that the elastic stress decreased by about 10 Pa during band formation in PBZT solutions. And, although strain recovery up to around four strain units has been observed for lyotropic LCPs,[58] based on the geometry of reorientation, an order of magnitude of 0.1 for strain recovery is much more appropriate. Therefore, an approximate order of magnitude for W is about 100 N/m^2. Moreover, a value of 0.1 for ψ produces a reorientation of around 20°, which is typical of banded textures in lyotropic LCP films. Combining these parameters produces a characteristic length of about 700 nm and a band spacing of about 14 μm. This is at least the correct order of magnitude for the spacing of banded textures observed in lyotropic systems (4−20 μm). Thus, the model describes the features of banded textures in a manner that is at least qualitatively correct.

Although these results are quite basic, they demonstrate the importance of incorporating the dynamics of director reorientation in theoretical and experimental research involving banded texture formation in LCPs. It should also be pointed out that equations quite similar to the ones derived here could result from a number of instability mechanisms in nematics.[59] Therefore, the development of the means to link the predictions of pattern formation theories with experimental results should provide a better understanding of this phenomenon, and could prove to be a vital ingredient in strategies to control and improve the structure and resulting properties of LCP materials and products.

5. Conclusions

A new model has been developed which sheds significant light on the problem of the formation of banded

textures in LCPs after high-speed flow. For the first time, the mechanism by which stress relaxation can lead to the formation of stable periodic structures has been established from first principles by considering the effects of strain recovery in combination with extended Frank elasticity on the reorientation dynamics of LCPs. Moreover, analysis of the model shows that this mechanism is active only when a key dimensionless parameter in the model exceeds a critical value, a situation which can occur only when a suitably large persistence length is combined with a significant compressive elastic modulus. This explains why banded textures are present in LCPs but not small molecule liquid crystals or flexible polymers. The effect of various forms of elastic anisotropy on the characteristics of the periodic patterns which form has also been examined, with the results demonstrating that the model predicts the correct shape and orientation of the bands in main-chain LCPs. In addition, the band spacing, which can be predicted using the model, agrees qualitatively with experimental observations. Finally, the model is able to describe the experimentally observed formation of bands through anisotropic domain growth, thus it retains the useful features of existing models while representing a significant forward step in the understanding of pattern formation in LCPs.

Acknowledgment. The authors would like to acknowledge the support of the National Science Foundation (Grant DMR 99-03519), and the Ohio Board of Regents for this work.

References and Notes

(1) For an excellent review, see Viney, C.; Putnam, W. S. *Polymer* **1995**, *36*, 1731−1741.
(2) Donald, A. M.; Windle, A. H. *J. Mater. Sci.* **1983**, *18*, 1143−1150.
(3) Viney, C.; Donald, A. M.; Windle, A. H. *Polymer* **1985**, *26*, 870−878.
(4) Viney, C.; Windle, A. H. *Polymer* **1986**, *27*, 1325−1331.
(5) Lee, K. G.; Barton, R.; Schultz, J. M. *J. Polym. Sci., Polym. Phys.* **1995**, *33*, 1−14.
(6) Wang, J.; Labes, M. M. *Macromolecules* **1992**, *25*, 5790−5793.
(7) Ernst, B.; Navard, P.; Haudin, J. M. *J. Polym. Sci., Polym. Lett.* **1987**, *25*, 79−82.
(8) Plummer, C. J. G.; Zuelle, B.; Demarmels, A.; Kausch, H. H. In *Deformation, Yield and Fracture of Polymers: Conference Proceedings*; PRI: Cambridge, England, 1991; pp 88/1−88/4.
(9) Kiss, G.; Porter, R. S. *Mol. Cryst. Liq. Cryst.* **1980**, *60*, 267−280.
(10) Donald, A. M.; Viney, C.; Windle, A. H. *Polymer* **1983**, *24*, 155−159.
(11) Horio, M.; Ishikawa, S.; Oda, K. J. *J. Appl. Polym. Sci., Appl. Polym. Symp.* **1985**, *41*, 269−292.
(12) Li, L. S.; Allard, L. F.; Bigelow, W. C. *J. Macromol Sci.* **1983**, *B22*, 269−290.
(13) Navard, P. *J. Polym. Sci., Polym. Phys.* **1986**, *24*, 435−442.
(14) Navard, P.; Zachariades, A. E. *J. Polym. Sci., Polym. Phys.* **1987**, *25*, 1089−1098.
(15) Peuvrel, E.; Navard, P. *Macromolecules* **1991**, *24*, 5683−5686.
(16) Shimamura, K. *Makromol. Chem., Rapid Commun.* **1983**, *4*, 107−111.
(17) Zachariades, A. E.; Logan, J. A. *Polym. Eng. Sci.* **1983**, *23*, 797−803.
(18) Zachariades, A. E.; Navard, P.; Logan, J. A. *Mol. Cryst. Liq. Cryst.* **1984**, *110*, 93−107.
(19) Vermant, J.; Moldenaers, P.; Mewis, J.; Picken, S. J. *J. Rheol.* **1994**, *38*, 1571−1589.
(20) Krause, S. J.; Vezie, D. L.; Adams, W. W. *Polym. Commun.* **1989**, *30*, 10−13.
(21) Kerkam, K.; Viney, C.; Kaplan, D. L.; Lombardi, S. J. *Nature* **1991**, *349*, 596−598.
(22) Nishio, Y.; Takahashi, T. *J. Macromol. Sci.* **1985**, *B23*, 483−495.
(23) Fischer, H.; Keller, A.; Windle, A. H. *J. Non-Newtonian Fluid Mech.* **1996**, *67*, 241−268.
(24) Romo-Uribe, A.; Lemmon, T. J.; Windle, A. H. *J. Rheol.* **1997**, *40*, 1117−1145.
(25) Jaffe, M. *Polym. Prepr.* **1999**, *40*, 574−575.
(26) Carri, G. A.; Muthukumar, M. *J. Chem. Phys.* **1998**, *109*, 11117−11128.
(27) Chen, F. L.; Jamieson, A. M. *Macromolecules* **1994**, *27*, 1943−1948.
(28) Odell, J. A.; Ungar, G.; Feijoo, J. L. *J. Polym. Sci., Polym. Phys.* **1993**, *31*, 141−155.
(29) Lonberg, F.; Fraden, S.; Hurd, A. J.; Meyer, R. B. *Phys. Rev. Lett.* **1984**, *52*, 1903−1906.
(30) Chang, S.; Han, C. D. *Macromolecules* **1996**, *29*, 2383−2391.
(31) Lonberg, F.; Meyer, R. B. *Phys. Rev. Lett.* **1985**, *55*, 718−721.
(32) Alderman, N. J.; Mackley, M. R. *Faraday Discuss. Chem. Soc.* **1985**, *79*, 149−160.
(33) Takebe, T.; Hashimoto, T.; Ernst, B.; Navard, P.; Stein, R. S. *J. Chem. Phys.* **1990**, *92*, 1386-1396.
(34) Srinivasarao, M.;. Berry, G. C. *J. Rheol.* **1991**, *35*, 379−397.
(35) Frank, F. C. *Trans. Faraday Soc.* **1958**, *25*, 19−42.
(36) Dobb, M. G.; Johnson, D. J.; Saville, B. P. *J. Polym. Sci., Polym. Phys.* **1977**, *15*, 2201−2211.
(37) Chu, B.; Ying, O.; Wu, C.; Ford, J. R.; Dhadal, H. S. *Polymer* **1985**, *26*, 1408−1418.
(38) Wang, X. Y.; Guenthner, A. J. *Phys. Rev. Lett.* **1999**, *82*, 4252−4255.
(39) Chandrasekhar, S. In *Liquid Crystals*, 2nd ed.; Cambridge University Press: New York, 1992; pp 362−367.
(40) Coullet, P.; Elphick, C.; Repaux, D. *Phys. Rev. Lett.* **1987**, *58*, 431−434.
(41) van Saarloos, W. *Phys. Rev. A* **1988**, *37*, 211−229.
(42) Peletier, L. A.; Troy, W. C. *SIAM J. Math. Anal.* **1997**, *28*, 1317−1353.
(43) Fisher, R. A. *Ann. Eugenics* **1937**, *7*, 355−369.
(44) Dee, G.; Langer, J. S. *Phys. Rev. Lett.* **1983**, *50*, 383−386.
(45) Ben-Jacob, E.; Brand, H. R.; Dee, G.; Kramer, L.; Langer, J. S. *Physica* **1985**, *14D*, 348−364.
(46) van Saarloos, W. *Phys. Rev. A* **1989**, *39*, 6367−6390.
(47) Wang, X. Y.; Fan, S.; Kyu, T. *Phys. Rev. E* **1997**, *56*, R4931−R4934.
(48) Aronson, D. G.; Weinberger, H. F. *Adv. Math.* **1978**, *30*, 33−76.
(49) Windle, A. H. In *Liquid Crystalline and Mesomorphic Polymers*; Shibaev, V. P., Lam, L., Eds.; Springer-Verlag: New York, 1994.
(50) de Gennes, P. G. *Mol. Cryst. Liq. Cryst. Lett.* **1977**, *34*, 177−182.
(51) Gunton, J. D.; San Miguel, M.; Sahni, P. S. In *Dynamics of First-order Phase Transitions*; Domb, C., Lebowitz, J. L., Eds.; Academic Press: New York, 1984; Vol. VIII.
(52) Picken, S. J.; Moldenaers, P.; Berghmans, S.; Mewis, J. *Macromolecules* **1992**, *25*, 4759−4767.
(53) DuPre, D. B. In *Polymer Liquid Crystals*; Ciferri, A., Krigbaum, W. R., Meyer, R. B., Eds.; Academic Press: New York, 1982.
(54) Grosberg, A. Y.; Zhestkov, A. V. *Polym. Sci. USSR* **1986**, *28*, 97−104.
(55) Romo-Uribe, A.; Windle, A. H. *Proc. R. Soc. London, A* **1999**, *455*, 1175−1201.
(56) Donald, A. M. *Polym. Commun.* **1986**, *27*, 18−20.
(57) Sato, T.; Teramoto, A. *Macromolecules* **1996**, *29*, 4107−4114.
(58) Moldenaers, P.; Mewis, J. *J. Rheol.* **1993**, *37*, 367−380.
(59) Zimmermann, W. *Phys. Rev. Lett.* **1991**, *66*, 1546.

MA9921448